4.5 **Idealized Three-Dimensional Simulations of Fronts Interacting with the U.S. West Coast Topography**

Joseph B. Olson* and Brian A. Colle

Institute for Terrestrial and Planetary Atmospheres, Stony Brook University / SUNY

1. INTRODUCTION

The coastal region of western North America frequently experiences intense orographically-enhanced wind and rainfall during the cool season. The steep coastal terrain in this region has been shown to cause upstream deceleration and deflection of the incident flow, thus producing strong terrain-parallel flow (barrier jet) at low-levels, and frontogenesis upstream of the barrier (Doyle, 1997; Colle et. al., 2002; Yu and Smull, 2001, among others).

This study uses the Penn State/NCAR mesoscale model (MM5) in an idealized configuration to investigate the structural development of the barrier jet along the U.S. West Coast and the interaction of landfalling systems with the barrier jet. The MM5 is nested down to 6-km grid spacing around the northern California coast in order capture the structural changes of the front approaching the coast and inland terrain. Various idealized terrain geometries are also explored to demonstrate the effect of terrain width on the landfalling systems.

For this study, an analytical initialization scheme has been developed for the MM5, which creates a semi-mature baroclinic wave with cold and warm fronts along with a characteristic westward tilt with height. This initialization scheme allows the flexibility to explore the full phase-space and evolution of the atmospheric frontal systems as they interact with the specified coastal terrain.

Some questions this study attempts to address are the following:

- What is the impact of the West Coast terrain on frontal structure and speed?
- What is the impact of different terrain geometries on the barrier jet and frontal interaction?
- What are the diabatic impacts of precipitation and surface fluxes on the landfalling front?

2. METHODOLOGY

a. Model Configuration

The MM5 was configured for three domains: 54, 18, and 6 km, using one-way nesting (Fig. 1a). Each domain consisted of 32 full sigma levels in the vertical. The coarse domain is large in the zonal direction so a variety of basic states and cyclone structures with varying phase speeds could be used without the cyclone entering or leaving the domain. This allows the lateral boundary conditions to be set constant for the outer domain.

The model physics were simplified to exclude moisture and surface fluxes. Only land or water values were used, with all land values set to coniferous forest. The Blackadar planetary boundary layer scheme (Zhang and Anthes 1982) was used to parameterize the turbulent and frictional effects of lower atmosphere. The diurnal variation of the radiation was also excluded. The radiative upper boundary condition was used to reduce the reflection of gravity waves from the model top at 100 mb.

b. Idealized baroclinic wave initialization

A version of a technique for generating analytical initial conditions of a three-dimensional baroclinic wave, originally developed by Fritsch et al. (1980) and further developed by Nuss and Anthes (1987), is used. This technique combines trigonometric functions with meteorological constraints to construct an idealized developing cyclone with vertical and horizontal structures typically found in the atmosphere. This method is similar to the original baroclinic wave initialization scheme in that it produces a cyclone structure tilting westward with height, a jet max located at the base of the upper level trough and a realistic tropopause geometry. Our modifications include an initial structure that is more developed at low-levels; therefore, less development is needed before terrain interaction occurs so we maximize control of the phase space.

The initialization procedure first consists of specifying a 2-dimensional pressure wave at 4-km, along with the full 3-dimensional temperature field in metric coordinates, with maximum amplitude of

* Corresponding author address: Joseph Olson, Marine Sciences Research Center, SUNY Stony Brook, NY, 11794-5000. email: joseph.olson@msrc.sunysb.edu

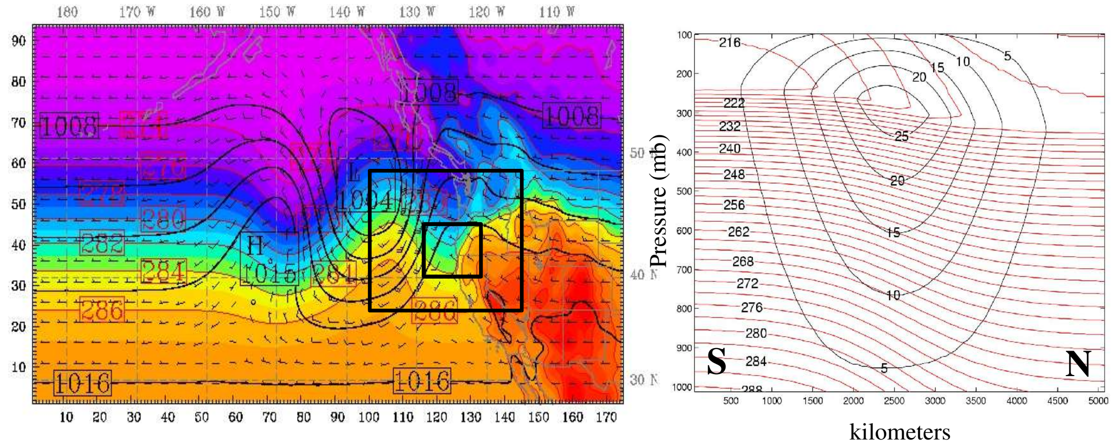

Figure 1. (a) Idealized baroclinic wave initialization from the 54-km grid with 18- and 6-km nests centered over steep coastal terrain. (b) Meridional cross-section of basic state temperature taken across the western portion of the coarse domain where the flow is zonal (red contours; 2 K interval) and wind (black contours; 5 m·s^{-1} interval) .

the zonally oriented wave perturbation in the mid and upper troposphere. Using the hydrostatic equation, we then integrate from the 4-km pressure level both upward and downward, to obtain the full 3-dimensional pressure field. The gradient wind approximation was used to calculate the winds after the three dimensional pressure field was transformed into geopotential height on a vertical pressure coordinate. These initial fields were used as input to the MM5 V3.5. More details can be found in the above references.

The parameters used to specify the strength of the basic state meridional temperature gradient and jet strength differed from Fritsch et al. (1980) and Nuss and Anthes (1987) so that the basic state was more similar to the average observed meridional temperature distribution over the eastern Pacific Ocean during the cool season (National Climatic Data Center online archive), with a north-south domain temperature difference of 18˚C over 5000 km, centered in the mid-latitudes. This yielded a jet maximum of about 30 ms^{-1} at 250 mb. The vertical temperature lapse-rate was set 6.5 °C km^{-1} but varies meridionally such that it is 0.2 ˚C larger (smaller) at the southern (northern) boundary. This specified lapse rate resulted in a mean Brunt-Vaisala frequency of N=0.012 s^{-1}. Figure 1b shows a meridionaly oriented vertical cross-section of the basic state initialized for these experiments upstream of the baroclinic wave. The shape of the tropopause was specified with a hyperbolic tangent function in the meridional direction and also varies in the zonal direction over the temperature wave, such that the height varies proportionally to the temperature wave. This results in a localized 50 mb depression of the tropopause over the upper-level trough and an upper-level potential vorticity anomaly.

c. Experiment design

Eight idealized simulations are conducted: four simulations with a baroclinic wave initialized and four simulations with zonal flow. The zonal simulations were performed to diagnose the response of westerly flow impinging on the various types of barriers and the baroclinic wave simulations were performed to show how variations in the terrain-forced flow affect the landfalling fronts. For each of these two groups of simulations, four different types of terrain were used: real mountains (REALM), idealized ridge (IDEALR), idealized plateau (IDEALP), and no terrain (NOTER). The idealized terrain was created in order to test the dependence of the terrain-forced flow on the barrier width and to help simplify the analysis. The idealized ridge was specified as a sine-squared slope similar to Williams et al. (1992) and the idealized plateau used the same slopes but were seperated by a zonal width of 1000 km. Both idealized terrain types were oriented north-south with a length of 2500 km and were positioned such that their western slopes coincided with the coasts of northern California and Oregon.

3. EVOLUTION OF THE LANDFALLING COLD FRONT

For simulations including the baroclinic wave, the low-level cyclone is initialized approximately 1200 km upstream of the coast (Fig. 2a). The initial cyclone structure is that of an open wave, which tilts westward with height. By hour 12 of the simulation (Fig. 2b), the idealized cyclone has deepened 2 mb and moved approximately 500 km eastward. The low-level flow deformation associated with the cyclone intensification acts to

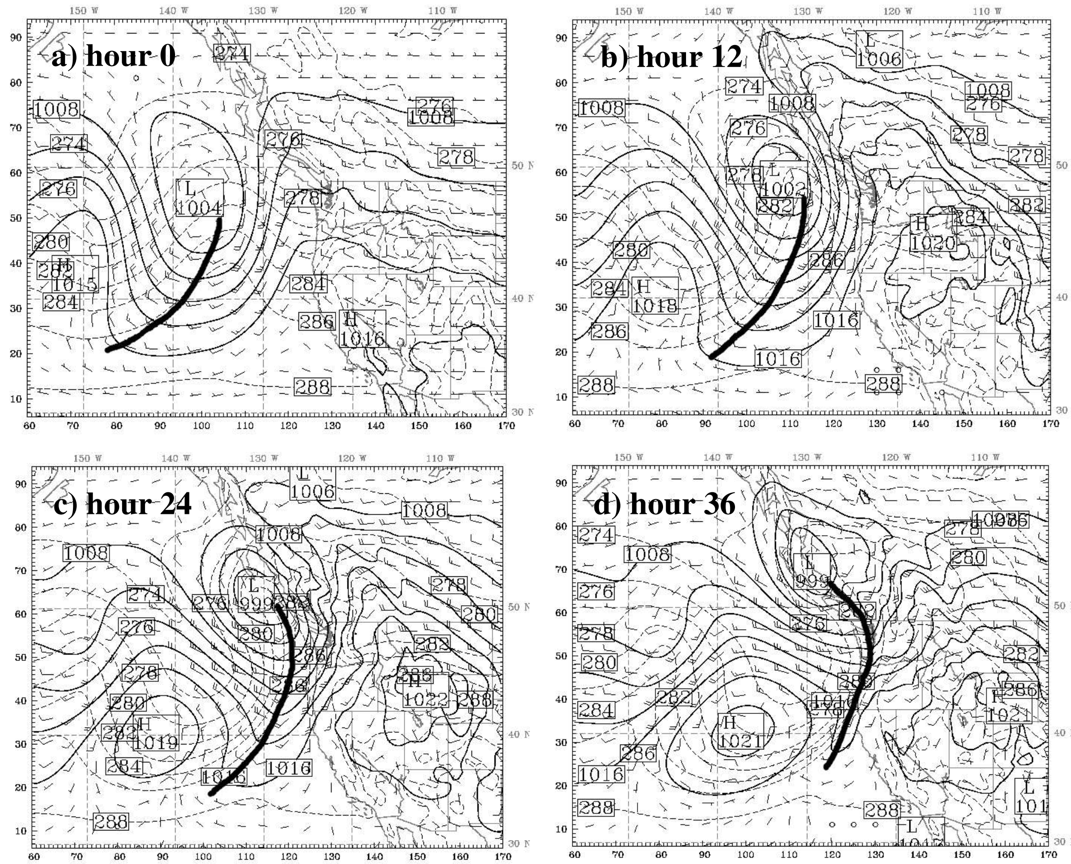

Figure 2. Synoptic evolution of the landfalling front from the 54-km domain at (a) hour 0, (b) hour 12, (c) hour 24, and (d) hour 36. Sea-level pressure (solid black contours; intervals of 2 mb), temperature (dashed grey contours; intervals of 2 °C), and wind (full barb = 10 knots).

enhance the cold front. Meanwhile, a ridge has developed over western North America.

At hour 24 (Fig 2c), ridging over the mountainous regions and the occlusion of the surface cyclone resulted in a northward deflection of the landfalling cyclone. The cyclone had continued to deepen another 3 mb. The cold front is positioned approximately 300 km upstream of the coast.

At hour 31 the cyclone has occluded and is making landfall. Strong terrain-parallel flow is evident along the coastal region of northern California (Fig. 3a). The cold front is approximately 100 km upstream of the coast and is already interacting with the terrain-forced flow. Figure 3b shows the hour 28 surface analysis of the NOTER simulation, which has the front in approximately the same position, but the prefrontal flow is about 5-10 $m \cdot s^{-1}$ weaker and oriented more southwesterly.

The difference between REALM and NOTER can be quantified by comparing vertical cross-sections of the front, taken at the bold black line seen in Fig. 3a (Fig. 4), for the same times chosen in Fig 3. For the averaged simulated values over the lowest 12 sigma levels of zonal wind, $U=10\ m \cdot s^{-1}$, $N=0.012\ s^{-1}$, and mountain height, $H_M=1800$ m. This yields a Froude number of 0.46, which is in the moderate blocking regime. In the cross-section for REALM (Fig. 4a), the low-level blocking results in the formation of the barrier jet with maximum strength of 16 $m \cdot s^{-1}$ near the top of the planetary boundary layer. This barrier jet has interacted with the front and caused a collapse in the frontal temperature gradient at hour 31. The NOTER solution (Fig. 4b), with no barrier jet, shows a much weaker front at hour 28.

At hour 36 of the simulation, the cyclone has moved inland and was experiencing cyclolysis (Fig. 2d). The cold front has slowed, weakened, and distorted by the terrain. At the southern flank of the cyclone, the cold front is very shallow and therefore, becomes trapped at the coast. Throughout the rest of the simulation, this blocking of the front south of 40°N, results in cold frontal deformation. In the no-terrain simulation, the front can be seen approximately 800 km further downstream by hour 48 (not shown).

c. Zonal flow simulations

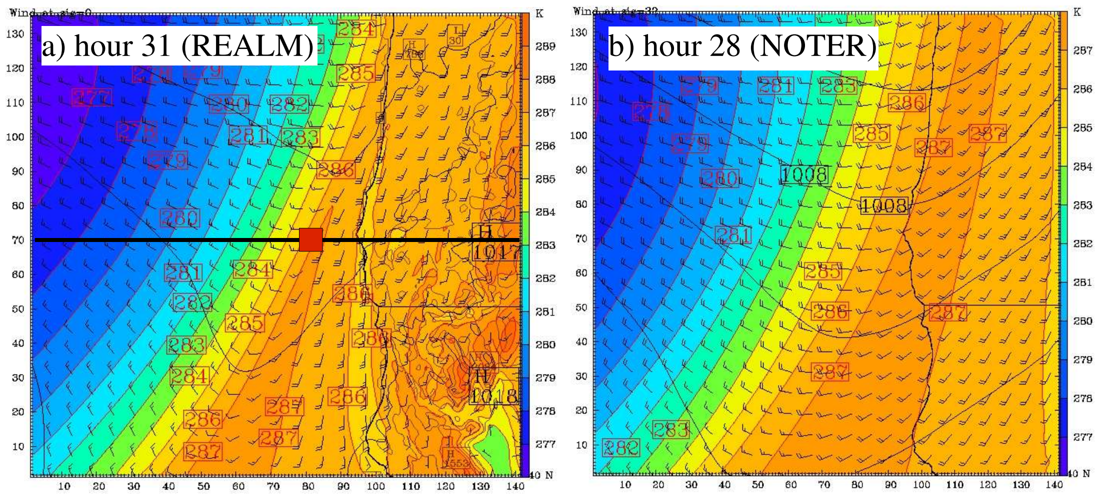

Figure 3. (a) Surface analysis from the 6-km nest at hour 31 of the REALM simulation and (b) hour 28 of the NOTER simulation. Sea-level pressure (black contours; intervals of 2 mb), potential temperature averaged over lowest 4 sigma level (colored), and winds (black barbs) also averaged over lowest 4 sigma levels.

The development of the terrain-forced flow has been shown by Braun et al. (1999) using 2-D simulations, to be dependent upon the barrier width. We explored this further in the 3D MM5 by running zonal simulations (same basic state as baroclinic wave experiments but with no wave initialized). At hour 24 (Fig. 5), the barrier jet is at approximately maximum strength for all three zonal terrain experiments: IDEALR (Fig 5a) has maximum speed of 9 m·s^{-1}, IDEALP (Fig. 5b) has maximum speed of 11 m·s^{-1}, and REALM (Fig. 5c) has max speed of 9 m·s^{-1}. The difference between the ridge and the plateau are threefold: 1) the barrier jet maximum is 2 m·s^{-1} larger in the plateau simulation. 2) the terrain-forced flow extends further upstream, and 3) the terrain-forced flow extends deeper into the troposphere for the plateau. This variation of the terrain-forced flow will be shown in the next section to result in variations in strength of the landfalling fronts.

4. FRONTAL ANALYSIS.

One important question to ask: Does the inland terrain play an important role on the rapid upstream frontogenesis observed during the landfall of cold fronts? To test how this upstream frontogenesis varies with barrier type, we performed idealized baroclinic wave simulations with idealized terrain. These simulations were then compared to the REALM simulation to show the significant effect of the inland terrain.

First, a comparison of the NOTER and REALM simulations were made to show the impact of terrain on the landfalling system. Figure 6 shows the time evolution of the potential temperature gradient simulated in 6-km domain

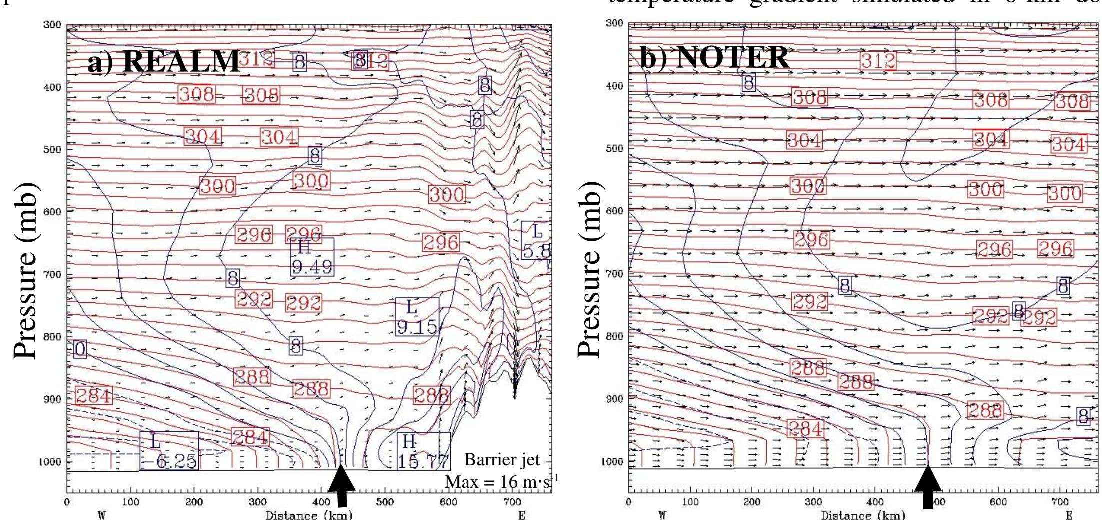

Figure 4. Cross-sections in 6-km domain showing potential temperature (red contours; 1 K interval), meridional wind (dark blue contours; intervals of 2 m·s^{1}), and circulation vectors (black vectors). Bold black arrows indicate the leading edge of front.

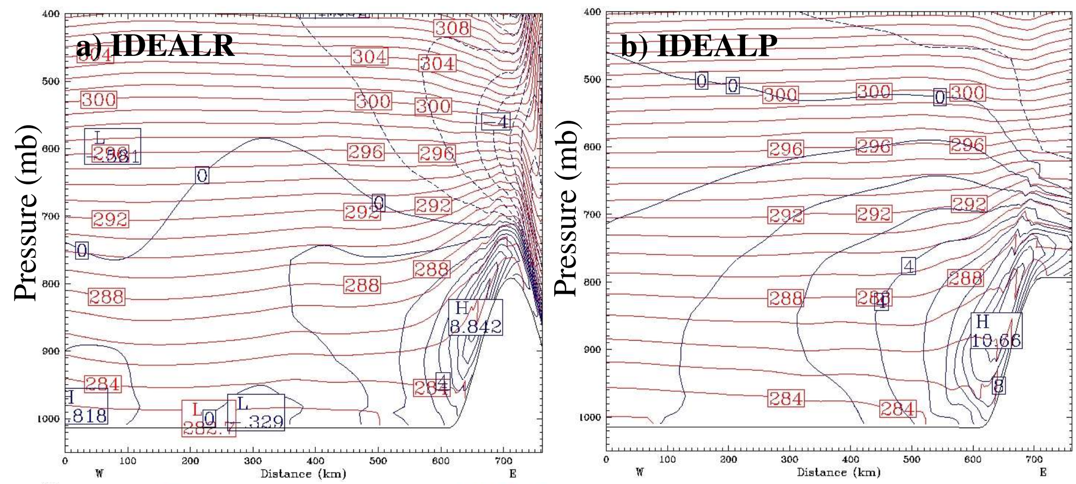

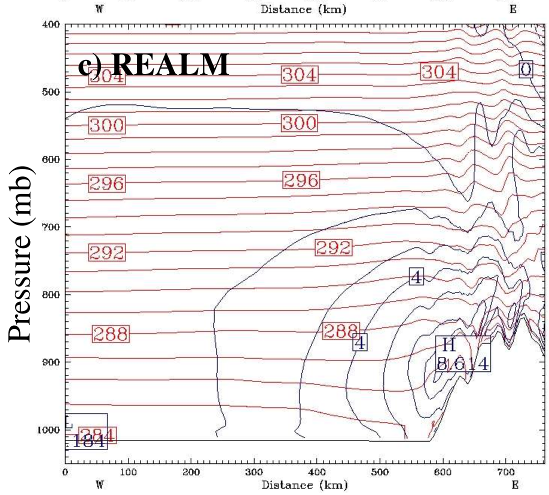

Figure 5. Meridional velocity (dark blue; every 1 m·s^{-1}) and potential temperature (red; every 1 K) for (a) idealized ridge (IDEALR), (b) idealized plateau (IDEALP), and (c)real terrain (REALM).

for both the NOTER (left) and REALM (right). This Hovmoller diagram was constructed for the same latitude used for the cross-section end points in Figs. 4 and 5. The color represents the absolute magnitude of the temperature gradient associated with the front in degrees K[100 km]$^{-1}$. Two main features are evident: 1) the front reaches the coast (grey line) three hours earlier in the NOTER simulation versus the REALM simulation and 2) the cold front begins to strengthen more rapidly in the REALM case as it reaches a temperature gradient of about 10 K[100 km]$^{-1}$ just prior to landfall.

Analysis of the upstream frontogenesis was conducted by averaging the absolute magnitude of the potential temperature gradient and the Miller Frontogenesis terms (Miller, 1948) over a three-dimensional volume following the front as it passed through the 6-km domain. This volume included a horizontal area of 7 by 7 grid and spanned the lowest 4 sigma levels. It is centered over the leading edge of the front and follows the front, along the same latitude as the Hovmoller diagrams (red box seen in Fig. 3a).

For simulated values of N=.012 s^{-1}, approximate mountain height H_M~1800 m, and

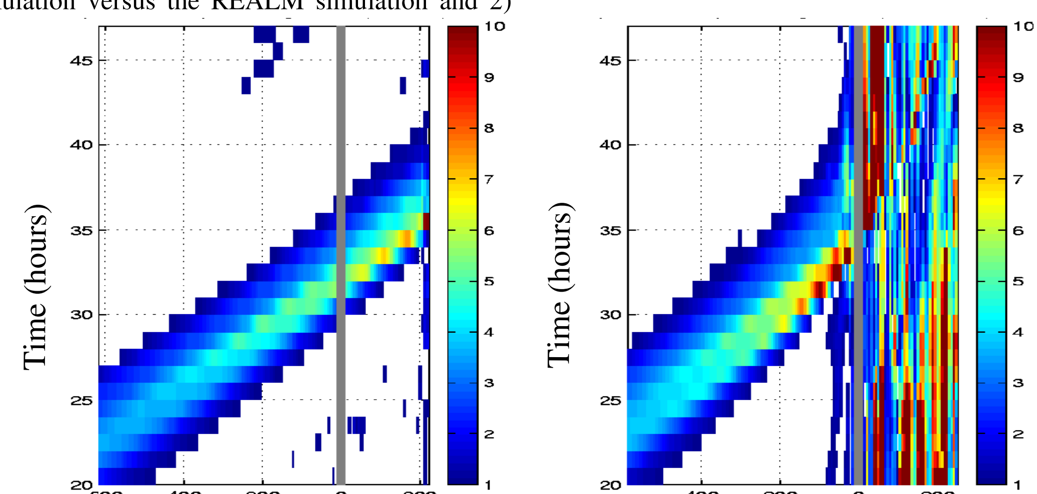

Figure 6. Time evolution of temperature gradient simulated at 6-km resolution; no terrain (left) and real terrain (right). The coast is represented by the grey line. Units in degrees K[100 km]$^{-1}$.

$f=10^{-4}$ s^{-1}, the Rossby radius of deformation (NH_M/f) is 220 km; therefore, the terrain forced flow extends approximately 220 km upstream of the coast. As the front enters this approximate distance from the coast (Fig. 7a), it begins to strengthen in the REALM case, while it experiences very little strengthening in the NOTER case. The front reaches a maximum of about 10 K[100 km]$^{-1}$ at the coast in the REALM case, but reaches a maximum inland in the NOTER case due to the increased friction at the coast.

The volume-averaged Miller frontogenesis terms for NOTER shows relatively no forcing west of the coast with only a very small increase after landfall (Fig. 7b). The upstream influence on the frontogenesis for the REALM case is controlled by the confluence and shear deformations (Fig. 7c), which increases approximately 220 km upstream of the coast. The tilting terms produces a small frontolytic response, but the magnitude of this term is less than 20% of the shear and confluence terms.

Volume averaged Miller frontogenesis was calculated for the baroclinic wave simulations using the idealized ridge (IDEALR) and plateau (IDEALP) geometries. Fig. 8 shows the Hovmoller diagrams constructed for the frontal interaction experiments with idealized terrain. Again, two main features are evident: 1) The front reaches the coast (grey line) two hours earlier in the IDEALR simulation than the IDEALP simulation and 2) The cold front begins to strengthen slightly further upstream in the IDEALP case as it reaches a temperature gradient of about 10 K[100 km]$^{-1}$ approximately 150 km upstream of the coast while the IDEALR case

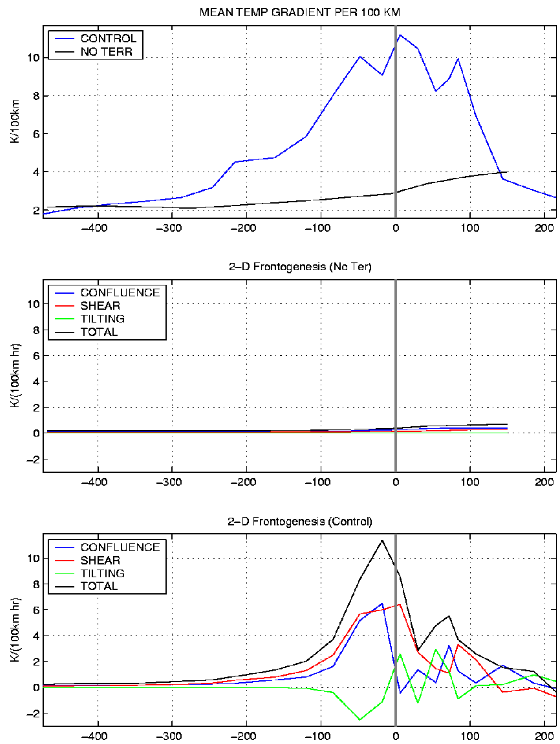

Figure 7. (a) Absolute magnitude of temperature gradient for REALM (control) and NOTER, as a function of distance from the coast, (b) Miller frontogenesis terms: confluence (blue), shear (red), tilting (green), and total (black) for no-terrain case, and (c) same as (b) but for terrain case.

reaches that magnitude at about 50 km from the coast.

As a final comparison between the two idealized barriers and the real topography of western North America, Fig. 9 shows the evolution of the horizontal potential temperature gradient as a function of distance from the coast. It is evident

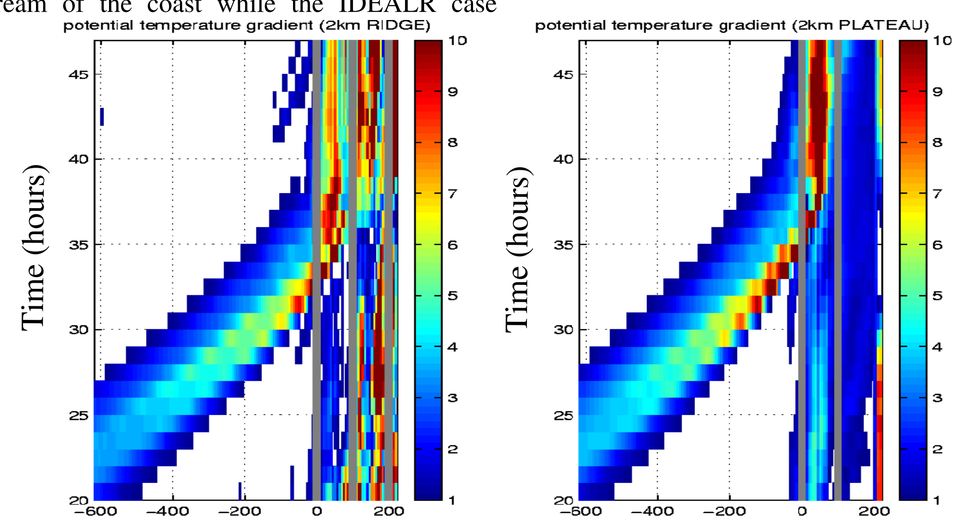

Figure 8. Time evolution of temperature gradient simulated at 6-km grid spacing, showing IDEALR (ridge case; left) and IDEALP (plateau case; right). The grey lines represent the coast (x=0), peak (x=100 km), and eastern edge of ridge (x=200 km). Units in degrees K[100 km]^{1}

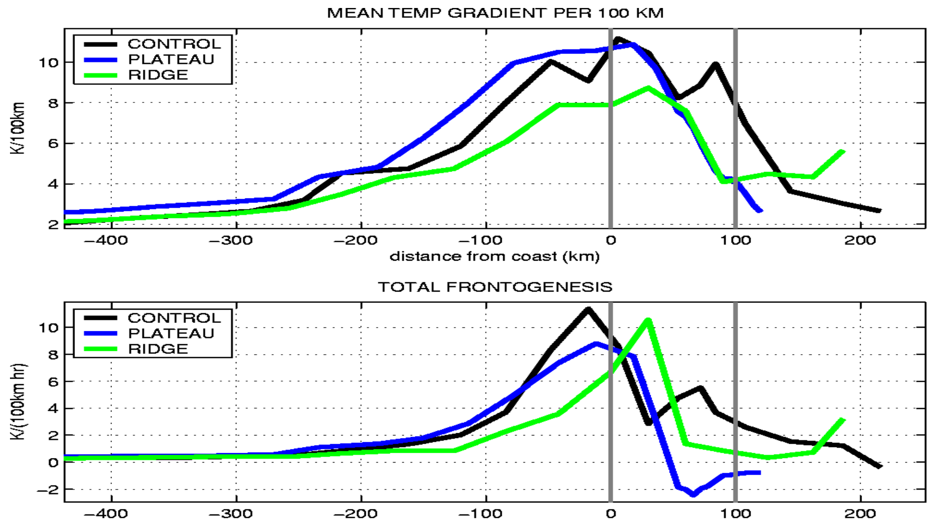

Figure 9. (a) absolute magnitude of potential temperature gradient as a function of distance from the coast and (b) total Miller frontogenesis terms. REALM (black), IDEALP (blue), and IDEALR (green).

that the upstream influence of the front caused by the real terrain (black) is more similar to that of the plateau (blue) than that of the ridge (green). The initial enhancement seen at around 220 km from the coast also appears in the plateau simulation but only increases slightly in the ridge simulation. Also, the maximum frontal strength of 10 K[100 km]$^{-1}$ seen in both the real terrain and plateau cases but the ridge case has a maximum of 8 K[100 km]$^{-1}$ at the coast. This similarity between the real terrain and the plateau also exists in the volume averages of the total Miller frontogenesis calculations (Fig. 9b). These results imply that the upstream influence of western North American topography on fronts is similar to a plateau response.

Summary

The idealized MM5 initialization/modeling set up is capable of producing many realistic features observed such as frontal retardation, rapid upstream frontogenesis, and a strong barrier jet. For the REALM simulation, the front doubled in magnitude as compared to the NOTER simulation near the coast. It was shown that the enhanced deformation caused by the terrain-forced flow led to the rapid upstream frontogenesis within a Rossby radius from the coast.

The variation of the structure of the terrain forced flow was shown to be dependent upon the width of the barrier. The plateau-like barrier generated a barrier jet 2 m·s^{-1} larger that the ridge-like barrier and the response extended further upstream and deeper into the troposphere. The inland terrain generates more of a plateau response, resulting in more upstream blocking and frontogenesis.

In the future, this work will be expanded upon to investigate the structural development and evolution of the barrier jets forced by the steep coastal terrain of western North America. Some specific aspects of this phase-space which need to be addressed are: the effects of precipitation, surface fluxes, and the dependence of the direction of the flow impinging on the barrier. Under these various forcings, the barrier jet and the landfalling cold fronts are likely to vary in both structure and strength.

Acknowledgments

This research is supported by the Office of Naval Research (Grant N00014-00-1-0407). Use of the MM5 was made possible by the Microscale and Mesoscale Meteorological Division at the National Center for Atmospheric Research, which is supported by the National Science Foundation.

References

Braun, S. A., Rotunno, Richard, Klemp, Joseph B. 1999: Effects of Coastal Orography on Landfalling Cold Fronts. Part I: Dry, Inviscid Dynamics. *Journal of the Atmospheric Sciences*: Vol. 56, No. 4, pp. 517–533.

Colle, Brian A., Smull, Bradley F., Yang, Ming-Jen. 2002: Numerical Simulations of a Landfalling Cold Front Observed during COAST: Rapid Evolution and Responsible Mechanisms*. *Monthly Weather Review*: Vol. 130, No. 8, pp. 1945–1966.

Doyle, James D., 1997: The Influence of Mesoscale Orography on a Coastal Jet and Rainband. *Mon.*

Wea. Rev., **125**, 1465-1488.

Fritsch, J. M., Magaziner, E. L., Chappell, C. F.. 1980: Analytical Initialization for Three-Dimensional Numerical Models**.** *Journal of Applied Meteorology*: Vol. 19, No. 7, pp. 809–818.

Miller, James E. 1948: On the Concept of Frontogenesis. *Journal of the Atmospheric Sciences*: Vol. 5, No. 4, pp. 169–171.

Nuss, Wendell A., Anthes, Richard A. 1987: A Numerical Investigation of Low-Level Processes in Rapid Cyclogenesis. *Monthly Weather Review*: Vol. 115, No. 11, pp. 2728–2743.

Schumann, U., 1987: Influence of Mesoscale Orography on Idealized Cold Fronts. *J. Atmos. Sci.*, 44, 3423-3441.

Yu, Cheng-Ku, Smull, Bradley F. 2000: Airborne Doppler Observations of a Landfalling Cold Front Upstream of Steep Coastal Orography. Monthly Weather Review: Vol. 128, No. 6, pp. 1577–1603.

Zhang, Dalin, Anthes, Richard A. 1982: A High-Resolution Model of the Planetary Boundary Layer —Sensit ivity Tests and Comparisons with SESAME-79 Data**.** *Journal of Applied Meteorology*: Vol. 21, No. 11, pp. 1594–1609.